Radio Science, Volume 12, Number 2, pages 311-317, March-April 1977

Multifrequency studies of ionospheric scintillations

R. Umeki, C. H. Liu, and K. C. Yeh

Department of Electrical Engineering, University of Illinois at Urbana-Champaign, Urbana, Illinois 61801

(Received September 1, 1976.)

Simultaneous scintillation data from the ATS-6 Radio Beacon Experiments for signals at 40, 140, and 360 MHz offer the opportunity to study the frequency dependence of the scintillation phenomenon. Using these data variations of the spectral index, correlation coefficient, and the correlation interval are investigated. It is found that for weak scintillations, the spectral indices lie between 1.5 and 1.7. When the scintillation is strong, the spectral indices vary from about 1.4 to 0.7. The correlation coefficients are found to decrease for increasing scintillation level. The interesting behavior of the correlation intervals as functions of signal frequency is also discussed. The observational results are compared with theoretical predictions.

1. INTRODUCTION

When a radio wave propagates through the ionosphere, the random irregularities present can cause the parameters of the wave to fluctuate. This is known as the ionospheric scintillation phenomenon. Because of its obvious relations to satellite communication systems and to the ionosphere physics, the phenomenon has been studied by many investigators in the past two decades or so [*Ratcliffe*, 1956; *Briggs and Parkin*, 1963; *Yeh and Swenson*, 1964; *Elkins and Papagiannis*, 1969; *Aarons et al.*, 1971; *Rufenach*, 1972; *Fremouw and Rino*, 1973; *Singleton*, 1974; *Crane*, 1976]. Early observations were made mostly at single frequencies. Since the fluctuations of the signal are caused by the irregular variations of the relative dielectric permittivity of the ionosphere and it is well known that such variations are inversely proportional to the square of the signal frequency, one would expect certain corresponding frequency dependence of the scintillation phenomenon. The radio beacon experiments on ATS-6, with the three frequencies at 40, 140, and 360 MHz, provide us with a good opportunity for simultaneous multifrequency observations of the scintillation phenomenon and allow us to study the frequency dependence of the various scintillation observables. In this paper, some results of our analysis of the ATS-6 scintillation data are presented, and we attempt to interpret the results in terms of the existing scintillation theories.

In section 2, we first discuss the data and the procedure to analyze them, and then present the results. The interpretations of the results are discussed in section 3, in which the observational findings are compared with the theoretical predictions. Some conclusions will be drawn from the comparison.

2. DATA ANALYSIS AND RESULTS

Linearly polarized radio signals were transmitted from the ATS-6 satellite (0°N, 94°W) at carrier frequencies of 40, 140, and 360 MHz. The amplitudes among other parameters of the signal were received in Boulder, Colorado (40.13°N, 105.24°W) by the Space Environmental Laboratory of the National Oceanic and Atmospheric Administration. The elevation angle was 42.2° at an azimuth of 162.9°. To guard against aliasing, the receiver has a post detection analog filter with a 1-sec time constant (0.16 Hz corner frequency) and single pole roll off (6 db/octave). After filtering, the signals were sampled at a rate of 10 Hz. Each second, ten of these 0.1-sec samples were averaged together and stored on magnetic tape via minicomputer. The final sampling rate was thus 1 Hz.

From the data, several periods where scintillation occurred were first located. A number of segments of the data which appeared stationary to the eye and were of sufficient time duration (at least 15 min) were chosen for analysis. A total number of 22 sets selected from data in the periods of August 21-24, December 24, 1974, and June 1-9, 1975, was

TABLE 1. Dates and times for data sets.

	Date	Time (UT)
Set I	12/24/74	0920-1000
Set II	1/9/75	0700-0750
Set III	8/23/74	0530-0545

analyzed. Of the 22 sets, three were picked for more detailed study. Their dates and times are given in Table 1. As an example of the data segments, Figure 1 shows the raw data for the three frequencies for data set II. Each data segment was subdivided into blocks of about 500 points. The mean and the scintillation index S_4 were computed for each block. The stationarity of the data was checked by verifying that both the mean and S_4 were relatively constant from block to block throughout the entire period being analyzed.

To detrend the data, we passed all points through a high-pass digital filter involving a weighted running mean of 400 data points. The detrended data were then used for computing the scintillation index, the autocorrelation function, the power spectrum, and the frequency correlation coefficients. Some of the results are presented in the following.

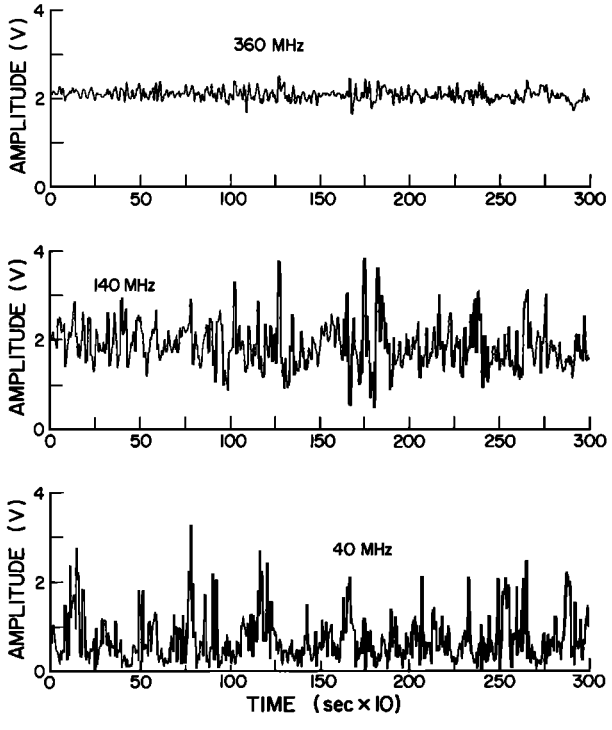

Fig. 1. Example of scintillation data at 40, 140, and 360 MHz.

TABLE 2. Scintillation and spectral indices.

Set	S_{4a}	S_{4b}	f_a	f_b	n
I	.54	.076	40	140	1.57
I	.076	.016	140	360	1.67
I	.54	.016	40	360	1.6
II	1.42	.54	40	140	.77
II	.54	.13	140	360	1.51
II	1.42	.13	40	360	1.09
III	.90	.31	40	140	.85
III	.31	.13	140	360	.92
III	.90	.13	40	360	.88

Table 2 shows the computed scintillation index S_4 and the spectral index n for data sets I, II, and III. The spectral index n is defined by

$$n(f_a/f_b) = \log(S_{4a}/S_{4b})/\log(f_b/f_a) \tag{1}$$

which gives the frequency dependence between the scintillation indices S_{4a}, S_{4b} at frequencies f_a and f_b respectively. We note that for data set I, the scintillation is relatively weak with S_4 ranging from 0.55 at 40 MHz to only 0.076 at 360 MHz. The spectral indices between the frequencies are approximately 1.6. Scintillation for set II is rather intense at 40 and 140 MHz. For this set, note the decrease of the spectral indices to 0.77 between 40 and 140 MHz and to 1.09 between 40 and 360 MHz. It is interesting to note that although the S_4 values in set III are not as high as those in set II, there is further decrease of the spectral indices for all frequencies for data set III.

To study further the dependence of the spectral index on the strength of scintillation, the results from all 22 sets were used to draw the histogram shown in Figure 2. The numbers shown inside each block indicate the average S_4 index at 140 MHz for the cases in that block. We note that there is a peak for spectral index n (140/40) in the interval 1.5-1.7. This peak corresponds to all the weak scintillation cases for which average $\bar{S}_4$ at 140 MHz is only 0.064. As scintillation strength increases, the spectral index decreases.

Next, we computed the cross-correlation coefficients between the frequencies using the formula

$$C\left(\frac{f_a}{f_b}\right) = \frac{\langle A_a A_b\rangle - \langle A_a\rangle\langle A_b\rangle}{[(\langle A_a^2\rangle - \langle A_a\rangle^2)(\langle A_b^2\rangle - \langle A_b\rangle^2)]^{1/2}} \tag{2}$$

where A_a and A_b are the amplitudes of the signals at frequencies f_a and f_b respectively. Table 3 shows

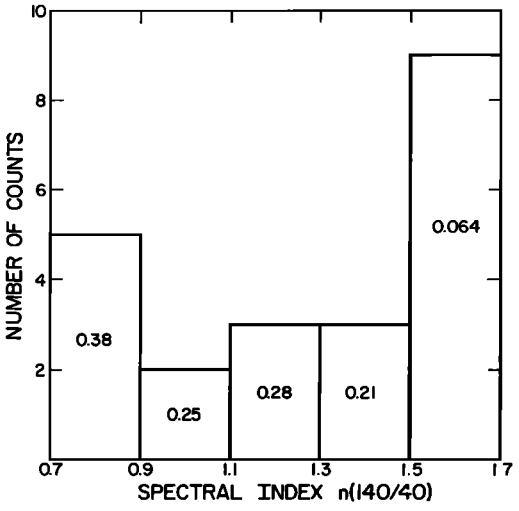

Fig. 2. Histogram for the spectral index $n(140/40)$.

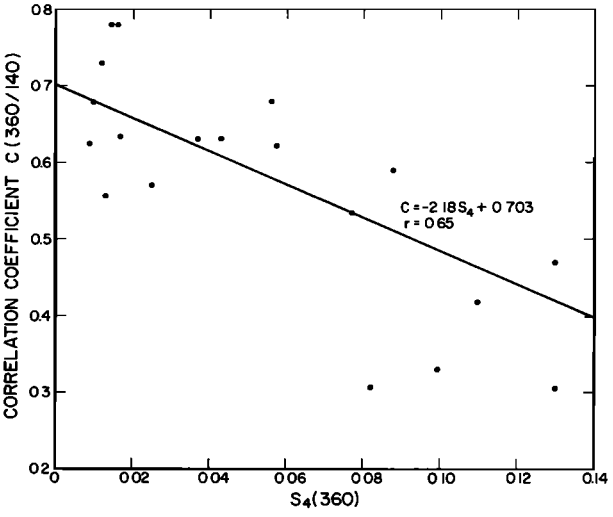

Fig. 3. Correlation coefficient between signals at 360 and 140 MHz as a function of the scintillation index S_4 at 360 MHz.

the mean correlation coefficients for all the cases studied. As expected, we see that as the difference between the frequencies widens, the correlation decreases. It is of interest here to also study how the correlation coefficients vary as the strength of scintillation increases. Figure 3 shows the variation of the correlation coefficient between 360 and 140 MHz as a function of scintillation index S_4 (360). The general trend of decreasing correlation for increasing S_4 is quite obvious from the scatter plot. When a regression line is fit through the data points, a slope of -2.18 is obtained. Figure 4 shows the same scatter plot for the correlation coefficients between 140 and 40 MHz as a function of S_4 at 140 MHz. The general trend of decreasing correlation for increasing S_4 is again apparent from the figure. However, when a regression line is fit through the points, a slope of -1.11 is obtained, indicating a slower change as compared to the case shown in Figure 3. Here, it is interesting to point out that the scintillation level for points in Figure 3 is much lower than that for points in Figure 4, ranging from 0.01 to 0.13 in the former case as compared to 0.06 to 0.55 in the latter case. Thus, the data seem to indicate that while in general the correlation coefficient decreases with increasing scintillation strength, the rate of change becomes slower as the level of scintillation grows. Indeed, a closer examination of Figure 4 indicates that for S_4 less than 0.2, the correlation coefficients seem to fall off at a faster rate than for those points corresponding to larger S_4 values. However, the results here have to be viewed with some caution. From (2) we note that the correlation coefficient becomes very sensitive to the contributions from

TABLE 3. Mean correlation coefficients.

$C(360/140)$	$C(140/40)$	$C(360/40)$
0.58	0.17	0.086

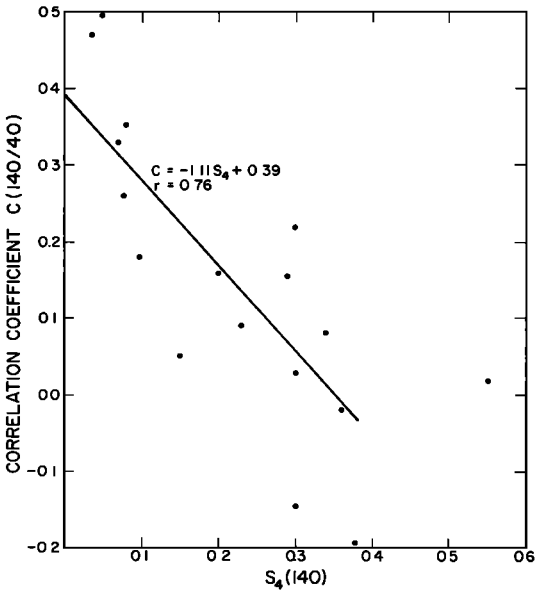

Fig. 4. Correlation coefficient between signals at 140 and 40 MHz as a function of the scintillation index S_4 at 140 MHz.

noise when the scintillation level is low. Therefore, the possibility that noise may be a contributing factor to this behavior cannot be ignored.

Figure 5 shows an example of the autocorrelation functions at the three frequencies computed from the data in set I. From the autocorrelation functions, we can obtain the correlation interval τ defined as the time interval between $R = 1$ and $R = 0.5$. For instance, the correlation intervals for data set I are $\tau(360) = 3.8$ sec, $\tau(140) = 4.8$ sec, and $\tau(40) = 7.5$ sec. It turned out that depending on the strength of scintillation, the relation among the correlation intervals for the three frequencies varies. To show this relation, we divide the 22 sets of data into four groups according to the values of scintillation indices at 360 MHz and the spectral indices $n(140/40)$ for the individual sets. The first group corresponds to the nine weak scintillation cases for which the $S_4(360)$'s are less than 0.02 and the mean spectral index $\bar{n}(140/40)$ is 1.6. With the correlation intervals at 40 and 140 MHz normalized with respect to the correlation interval at 360 MHz, curve one in Figure 6 shows decreasing correlation intervals with increasing frequency. For the second group of four cases, $S_4(360)$ lies between 0.02 and 0.06 with $\bar{n}(140/40) = 1.38$. The third group of seven cases has $S_4(360) > 0.08$ and $\bar{n}(140/40) = 0.93$. The fourth group contains only two cases with $S_4(360)$ equals 0.06 and 0.13 and $\bar{n}(140/40) = 0.91$. The behavior of the correlation intervals for those three groups are shown in curves 2, 3, and 4 of Figure 6 respectively. Curve 2 has behavior similar to that of curve 1 except that the increase of the correlation interval τ at the low-frequency end is much less than that for the first group. Curve 3 shows that, for fairly strong scintillation, τ first increases as the frequency increases from the lower end, and then it reaches a maximum before it decreases to unity at 360 MHz. For group 4, τ at 360 is greater than τ_{140} and τ_{40} with τ_{40} the smallest among the three. The two cases in this group both show rather strong scintillation levels. Also we note that although the four curves diverge at the low frequency end, their behaviors are quite similar in the high-frequency region of the figure.

Figure 7 shows how the actual correlation interval $\tau(360)$ varies as the scintillation strength increases. We see that for weak scintillations such that $S_4(360)$

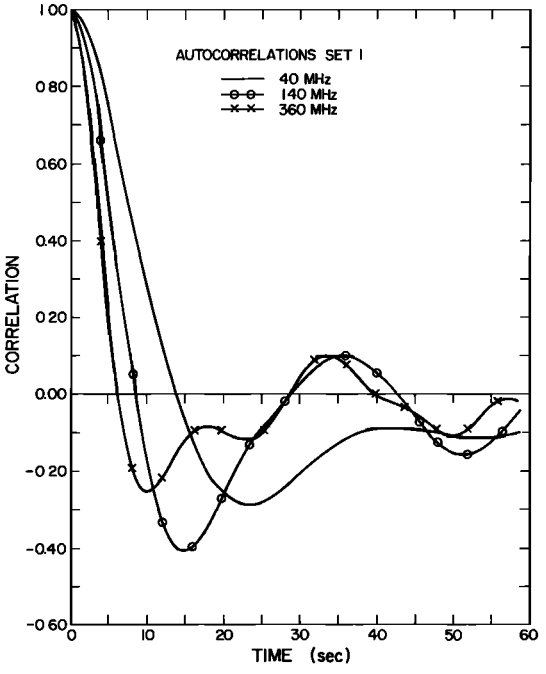

Fig. 5. Autocorrelation functions for data set I.

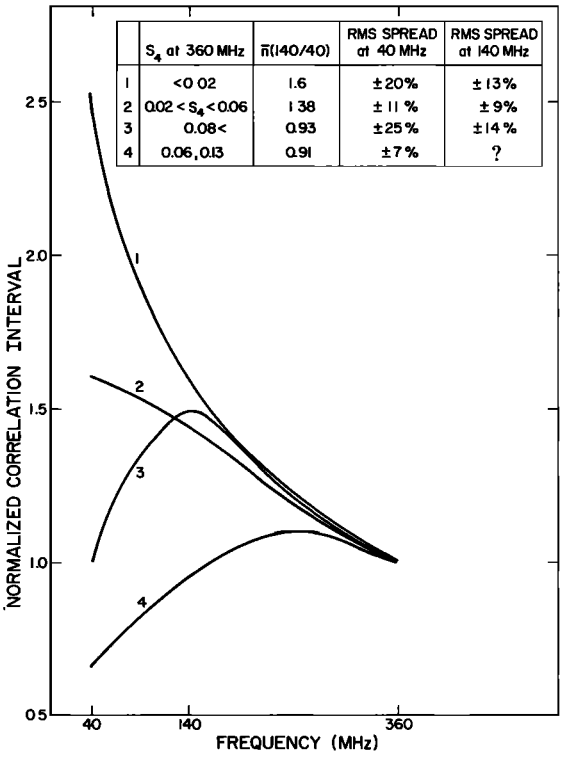

Fig. 6. Normalized correlation intervals as functions of signal frequency.

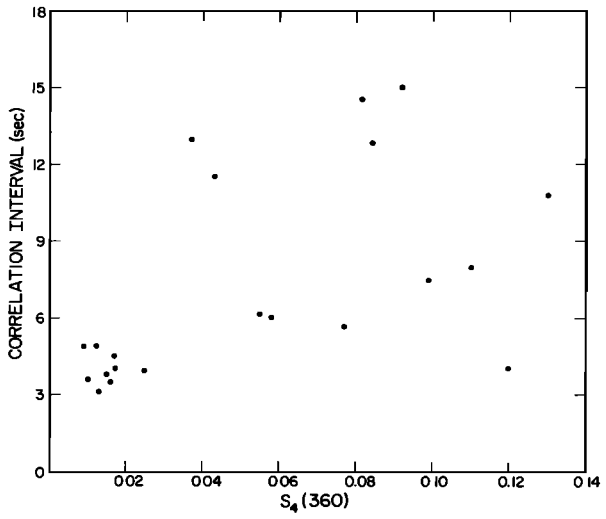

Fig. 7. Scatter plot for correlation intervals at 360 MHz vs. scintillation index S_4 at 360 MHz.

< 0.02, $\tau(360)$ lies in the range of 3~5 sec without much variation. As the scintillation strength grows, τ seems to increase. There is also much more variability in the correlation interval, ranging from 18 to about 4 sec.

3. DISCUSSION

In this section we attempt to interpret the results in section 2 in terms of the existing scintillation theories. Many authors have studied the ionospheric scintillation theory based on either thin phase screen [*Briggs and Parkin*, 1963], or Born approximation [*Budden*, 1965*a*], or Rytov approximation [*Wernik and Liu*, 1974]. Most of these investigations apply only to the case of weak scintillation. Previously, in an effort to interpret scintillation data using weak scintillation theory, care must be taken in selecting the data to ensure the applicability of the theoretical results [*Rino et al.*, 1976]. In the case of multifrequency observation, however, because of the fact that the random variation of the relative dielectric permittivity in the ionosphere is inversely proportional to the square of the signal frequency, under the condition for which only weak signal fluctuations occur at higher frequencies, signals at lower frequencies will suffer much more severe scintillations. Therefore, a unified scintillation theory that takes into account the effects of multiple scattering is necessary for the interpretation of the multifrequency data. Efforts to develop such a unified scintillation theory have just begun [*Liu et al.*, 1974; *Yeh et al.*, 1975]. Multifrequency scintillation data such as those obtained from ATS-6 are most valuable in the further development of the theory, for only through comparisons between theoretical predictions and observational results can the theoretical model be improved.

Let us begin with the results on scintillation index. Using weak scintillation theory, *Jokippi and Hollweg* [1970] showed that for a power-law irregularity spectrum of the form κ^{-p}, where κ is the spatial frequency (wavenumber) and p is the power index, the spectral index n for the scintillation index S_4 as defined in (1) is given by

$$n = (p + 2)/4 \tag{3}$$

Experimental evidence indicates a power-law irregularity spectrum in the ionosphere with a power index between 3.5 and 5 [*Rufenach*, 1972; *Dyson et al.*, 1974]; therefore, if the weak scintillation theory applies, (3) will predict a range of the spectral index approximately between 1.4~1.7, independent of the signal frequency. From Table 2, we see that n is about 1.6 for all three frequencies, well within the range predicted. Furthermore, from Figure 2, we see that for the nine cases for which the scintillations are weak with mean $S_4(360) = 0.064$, $n(140/40)$ lie between 1.5 and 1.7, leading to the range 4~4.8 for the power index p, again in fairly good agreement with previous observations. Therefore, it seems that for weak scintillation in the ionosphere, the existing weak scintillation theory predicts the frequency dependence of the scintillation index rather satisfactorily. On the other hand, using a multiple-scatter approach, *Yeh et al.* [1975] showed that for strong scintillations the spectral index depends on the strength of scintillation, and hence, on the frequency of the signal. We see from Table 3 that for data set II for which the scintillation is strong, the spectral index varies from 1.51 between 360 and 140 MHz to 0.77 between 140 and 40 MHz. Indeed, the spectral index depends on the signal frequency. This is due to the fact that when multiple scattering becomes important, saturation of the scintillation index occurs. Depending on how strong the multiple scattering is, the spectral index can vary from zero to the value given by (3). Figure 2 shows that the value of n decreases as the scintillation gets stronger, as predicated by the theory [*Yeh et al.*, 1975]. As a matter of fact,

there is some indication that the value of the spectral index may be as accurate an indication, if not better, of the importance of multiple scattering as that provided by the scintillation index S_4. Table 2 shows that for data set III, the scintillation indices range from 0.13 to 0.9 and the spectral indices range from 0.85 to 0.92. Although the scintillation indices are not as large as those for some other strong scintillation cases (such as set II), the fact that n remains rather small for all frequencies indicates the multiple scattering effects are very important for this set. That this is indeed the case will be seen later when we discuss the correlation intervals.

The cross-correlation coefficient between signals at different frequencies is an important quantity for communication system performance analysis as well as design of frequency diversity systems. Table 3 shows that the correlation coefficients decreases as the frequency separation between the signals increases. This is what one would expect. Figures 3 and 4 show that the correlation coefficient decreases with increasing scintillation strength as predicted by the weak scintillation theory [*Budden*, 1965*b*]. This is due to the fact that with more scattering, the signals become more decorrelated. However, as the scintillation strength grows, multiple-scattering effects become important. The signal undergoes many scatterings before it reaches the receiver and some sort of saturation effect occurs in the decorrelation process during the multiple-scattering process. Thus, for strong scintillation, the correlation coefficient does not decrease as fast with increasing S_4 as for weak scintillations. This result was qualitatively inferred by the computations of *Liu and Yeh* [1975].

In the theory of weak scintillation, the Fresnel zone plays a rather important role. The size of the Fresnel zone is given by $(\lambda z_0)^{1/2}$ where λ is the wavelength of the signal and z_0 is the distance from the center of the irregularity slab to the ground. Irregularities of the size of the Fresnel zone contribute most to the amplitude scintillation observed on the ground. Fresnel zone size also determines the correlation distance of the signals received on the ground. As the irregularities in the ionosphere drift across the signal path, temporal fluctuations of the signal are received on the ground as shown in Figure 1. For weak scintillation the correlation interval of the signal is approximately related to the Fresnel zone by

$$\tau = (\lambda z_0)^{1/2} / v \tag{4}$$

where v is the drift speed of the irregularities transverse to the radio path. Hence, we see that according to the weak scattering theory, the correlation interval of the scintillating signal should be inversely proportional to the square root of the signal frequency.

When the strength of scintillation increases, the correlation interval is no longer directly related to the size of the Fresnel zone. Since the multiple scattering now becomes effective, the signal is decorrelated. For a given ionospheric condition, the strength of scintillation increases as signal frequency decreases, thus for strong scintillations one would expect greater decorrelation, hence smaller correlation interval, as frequency decreases. Therefore, as far as the correlation interval is concerned, two competing processes exist. When the Fresnel filtering effect is more important, τ decreases as f increases. When the multiple scattering effect is dominant, τ increases as f increases. Under certain ionospheric conditions, a peak may appear as we plot τ as a function of f. *Yeh et al.* [1975] studied this problem for different ionospheric conditions and showed this behavior of τ as a function of signal frequency.

In Figure 6, note that for curves 1, 2, and 3 the high-frequency portions of the curves almost coincide with each other with an $f^{-1/2}$ variation as predicted by the weak scintillation theory. In this region the scintillation level is low for all the cases; therefore, the weak scattering theory applies. As we move to the low-frequency region where scintillation becomes stronger, we see a divergence of behavior for the different groups. Curve one still shows decreasing τ with increasing frequency, indicating the dominance of the Fresnel zone relation. However, multiple scattering may have already been somewhat effective at the low-frequency end, making the decrease of τ not quite as fast as $f^{-1/2}$. Curve 2 has the same behavior as curve 1. But now with stronger scintillation level, multiple scattering becomes more effective, resulting in even slower decay of τ as a function of f in the low-frequency region. For curve 3, scintillation at the low-frequency end is strong enough for the multiple scattering effect to be dominant in the region, while the scintillation level at the high-frequency end is still low enough for single-scatter theory to be valid.

Therefore, for this case we obtain a peaked curve for τ as a function of frequency, the result of the two competing processes mentioned above. For group 4, τ increases as f increases for the three frequencies, indicating that multiple scattering effects are dominant at all three frequencies. We note that for this group, although the scintillation indices are not particularly high, the spectral indices are quite low for all frequencies. Therefore, as we have discussed earlier, the low value of the spectral index seems to be a good indicator of the dominance of the multiple scattering effects.

Figure 7 shows the variation of the correlation interval for 360 MHz as a function of scintillation index. As mentioned above, at 360 MHz the scintillation level is low for all the cases so that the weak scattering theory is applicable. If we make the relatively reasonable assumption that the height of the irregularity slab does not vary much, then according to (4), the major cause of the variability of τ is the drift speed v. Figure 7 shows that for very weak scintillations, the drift speed does not vary much. When the scintillation level increases, the drift speed varies much more from case to case. There is also a general trend of decreasing drift speed with increasing scintillation level.

In this paper, we have presented some results of our analysis of the multifrequency scintillation data from the ATS-6 radio beacon experiments. In particular, we have concentrated on the frequency dependence of the amplitude scintillation, the spectral index, the cross correlation coefficient and the correlation interval of the signal. The experimental results are then interpreted by applying the existing scintillation theories. It turns out that the results agree, at least qualitatively, with the predictions from the multi-scatter scintillation theory.

Finally, we note that in addition to the results presented in this paper, computations of the power spectra, both for amplitude and phase, as well as the distributions of the amplitude and phase statistics were also made from the data. These will be subjects for future communications.

Acknowledgments. We thank K. Davies, R. F. Donnelly, R. N. Grubb, and R. B. Fritz of the Environmental Research Laboratories of the National Oceanic and Atmospheric Administration for making the ATS-6 data available to us. This work was supported by grants ATM 74-08765 and ATM 75-21755 from the Atmospheric Sciences Section of the National Science Foundation.

REFERENCES

Aarons, J., H. E. Whitney, and R. S. Allen (1971), Global morphology of ionospheric scintillation, *Proc. IEEE, 59*, 159-172.

Briggs, B. H., and I. A. Parkin (1963), On the variation of radio star and satellite scintillations with zenith angle, *J. Atmos. Terr. Phys., 25*, 330-366.

Budden, K. G. (1965*a*), The amplitude fluctuations of the radio wave scattered from a thick ionospheric layer with weak irregularities, *J. Atmos. Terr. Phys., 27*, 155-172.

Budden, K. G. (1965*b*), The theory of the correlation of amplitude fluctuations of radio signals at two frequencies, simultaneously scattered by the ionosphere, *J. Atmos. Terr. Phys., 27*, 883-897.

Crane, R. K. (1976), Spectra of ionospheric scintillation, *J. Geophys. Res., 81*, 2041-2050.

Dyson, P. L., J. P. McClure, and W. B. Hanson (1974), In-situ measurements of amplitude and scale size characteristics of ionospheric irregularities, *J. Geophys. Res., 79*, 1497-1502.

Elkins, T. J., and M. D. Papagiannis (1969), Measurement and interpretation of power law spectrum of ionospheric scintillation at subauroral location, *J. Geophys. Res., 74*, 4105-4115.

Fremouw, E. J., and C. L. Rino (1973), An empirical model for average *F*-layer scintillation at VHF/UHF, *Radio Sci., 8*, 213-222.

Jokippi, J. R., and J. V. Hollweg (1970), Interplanetary scintillation and the structure of solar-wind fluctuations, *Astrophys. J., 160*, 745-753.

Liu, C. H., and K. C. Yeh (1975), Frequency and spatial correlation functions in a fading communication channel through the ionosphere, *Radio Sci., 10*, 1055-1061.

Liu, C. H., A. W. Wernik, K. C. Yeh, and M. Y. Youakim (1974), Effects of multiple scattering on scintillation of trans-ionospheric radio signals, *Radio Sci., 9*, 599-607.

Radcliffe, J. A. (1956), Some aspects of diffraction theory and their application to the ionosphere, *Rep. Progr. Phys., 19*, 188-267.

Rino, C. L., R. C. Livingston, and H. E. Whitney (1976), Some new results on the statistics of radio wave scintillation, 1, Empirical evidence for gaussian statistics, *J. Geophys. Res., 81*, 2051-2058.

Rufenach, C. L. (1972), Power-law wave number spectrum deduced from ionospheric scintillation observations, *J. Geophys. Res., 77*, 4761-4772.

Singleton, D. G. (1974), Power spectra of ionospheric scintillations, *J. Atmos. Terr. Phys., 36*, 113-134.

Wernik, A. W., and C. H. Liu (1974), Ionospheric irregularities causing scintillation of GHz frequency radio signals, *J. Atmos. Terr. Phys., 36*, 871-879.

Yeh, K. C., and G. W. Swenson (1964), *F*-region irregularities studied by scintillation of signals from satellites, *J. Res. Nat. Bur. Stand. Sect. D, 68D*, 881-894.

Yeh, K. C., C. H. Liu, and M. Y. Youakim (1975), A theoretical study of the ionospheric scintillation behavior caused by multiple scattering, *Radio Sci., 10*, 97-106.